

AN ADAPTIVE CODE FOR RADIAL STELLAR MODEL PULSATIONS

J. ROBERT BUCHLER*, ZOLTÁN KOLLÁTH† and ARIEL MAROM

Physics Department, University of Florida, Gainesville, FL 32611

1. Introduction

The numerical hydrodynamical modelling of radial stellar pulsations goes back to the pioneering efforts of Christy (1966) in the mid 1960s. Reviews of the stellar pulsation problem can be found in the literature (*e.g.* Cox & Giuli 1969, Cox 1980, Buchler 1990). In our own past numerical work we have adopted the hydrodynamics code developed by Stellingwerf (1974, 1975) on the basis of Fraley's (1968) implicit Lagrangean scheme. This is a very stable and robust code, and in its relaxation version it is an excellent tool for computing periodic pulsations and their linear stability (Floquet analysis). The use of the code has produced good results for a variety of stellar models ranging from RR Lyrae (*e.g.* Stellingwerf 1975, Kovács & Buchler Kovács 1988a) and Cepheids (*e.g.* Moskalik, Buchler & Marom 1992) to irregularly pulsating variables (Kovács & Buchler 1988b), and good overall agreement with observations can be achieved. As these theoretical studies have progressed, and as more and better observational has accumulated it has become increasingly clear that a better code is needed (*e.g.* Buchler 1990) if further advances are to be made (Kovács 1990, Kovács & Buchler 1993).

In fact, right from the beginning of Cepheid modelling misgivings were expressed about the spatial resolution that can be obtained with a Lagrangean grid. The earliest adaptive attempts made to abate this deficiency were those of Castor, Davis & Davison (1977) and Aikawa & Simon (1983), Simon & Aikawa (1986), but these codes were not energy conserving. More recently, taking advantage of progress in numerical mathematics, a couple of efforts specifically aimed at stellar pulsations, and parallel to ours have been made (Dorfi & Drury 1987, Dorfi & Feuchtinger 1991, Feuchtinger & Dorfi 1994, Cox, Deupree & Gehmeyr 1992, Gehmeyr 1992a,b, 1993). The three codes differ in many respects,

* e-mail: buchler@phys.ufl.edu

† on leave from Konkoly Observatory, Budapest, Hungary



however. In particular, the other two codes solve the internal energy equation whereas we solve the total energy equation (While analytically these equations are equivalent, the tests that we describe below show that, numerically, the solution of the total energy equation is more accurate. Furthermore our grid equation while similar to Dorfi's uses a mass density rather than a radius density. A comparison of the three codes on a few standard stellar models would be desirable.

Our strategy in developing an adaptive code has been very conservative. Because of the success of the Stellingwerf-Fraley scheme we have decided to build an adaptive code on top of this Lagrangean scheme. By putting the mass and total energy equations in conservative form, and by properly defining the fluxes, we can write the adaptive scheme so that, *globally*, mass and total energy conservation are preserved. These constraints are essential for the stellar pulsation problem (*cf.* Buchler 1990; see also the tests below). Indeed, an examination of the energetics shows the pulsation to be rather delicate. The pulsation kinetic energy ($\approx 8 \times 10^{42}$ erg) is generally very small compared to both the gravitational energy ($\approx 8 \times 10^{47}$ erg) and the internal energy ($\approx 4 \times 10^{47}$ erg) which have opposite signs (from the virial theorem $2K + G \approx 0$). In addition, in the nonadiabatic case, the growth-rates are often small, *i.e.* it takes many pulsations to build up to the saturation amplitude. In contrast, the heat that flows through the stellar envelope in one pulsation ($\approx 2 \times 10^{43}$ erg) is very large (The indicated numerical values are for a typical classical Cepheid). The coupling of the pulsation to the heat-flux thus plays a very important role in the pulsations. It determines both the linear vibrational stability or instability and the saturation amplitude. Needless to say, it therefore requires an accurate difference scheme. One of the important checks is that in the linear regime the growth-rates obtained from the numerical hydrodynamics agree with those obtained from a linear stability of the normal modes of oscillation.

The prescription for converting to an adaptive mesh is well known (*e.g.* Winkler, Norman & Mihalis 1984). Three velocities appear, namely u , the physical velocity of the fluid with respect to a spatially fixed reference frame (here, the equilibrium stellar model), u_{grid} , the velocity of the mesh points with respect to the same reference frame and $u_{rel} = u - u_{grid}$ the fluid velocity relative to the mesh.

The adaptive mesh hydrodynamic equations, in their usual notation, are given by

$$\frac{d}{dt} \int \rho dV + \int \rho u_{rel} dA = 0 \quad (1)$$

$$\frac{\delta(\rho\Delta V)}{\delta t} + \Delta(\rho u_{rel}A) = 0 \quad (2)$$

$$\frac{d}{dt} \int u\rho dV + \int \rho u u_{rel} dA + \int \left(\frac{\partial p}{\partial r} + \rho \frac{GM}{r^2} \right) dV = 0 \quad (3)$$

$$\frac{\delta(u\rho\Delta V)}{\delta t} + \Delta(\rho u u_{rel}A) + A\Delta p + \frac{GM}{r^2} \rho\Delta V = 0 \quad (4)$$

$$\frac{d}{dt} \int \rho \left(e + \frac{u^2}{2} - \frac{GM}{r} \right) dV + \int \rho \left(e + \frac{u^2}{2} - \frac{GM}{r} \right) u_{rel} dA \quad (5)$$

$$+ \int (pu + F_L) dA = 0$$

$$\frac{1}{\delta t} \delta \left[\left(e + \frac{u^2}{2} - \frac{GM}{r} \right) \rho\Delta V \right] + \Delta \left[\left(e + \frac{u^2}{2} - \frac{GM}{r} \right) \rho u_{rel} A \right] \quad (6)$$

$$+ \Delta [(pu + F_L) A] = 0$$

where δ denotes the temporal change of a variable or expression and Δ the spatial variation. We treat the radiative flux in the diffusion approximation as we have done in the past with the Lagrangean code.

These equations have to be completed with a mesh equation which specifies how the mesh points are linked to the fluid. There is of course no universal prescription for a mesh equation, and we have adopted a variant of Dorfi & Drury (1987) which we shall describe in detail below.

In a separate paper we will relax the equilibrium diffusion approximation and add separate radiation equations.

2. The Code

Fraley's scheme is a staggered Lagrangean scheme in which the basic radii, velocities are defined at the cell edges (i), and the density and thermodynamic variables are defined at the cell centers ($i + \frac{1}{2}$) as shown in Figure 1.

Following common notation, each variable y_i^n is assigned a spatial subscript i (or $i + \frac{1}{2}$) and a temporal superscript n . Intermediate temporal values of the independent variables are defined with weights θ_y .

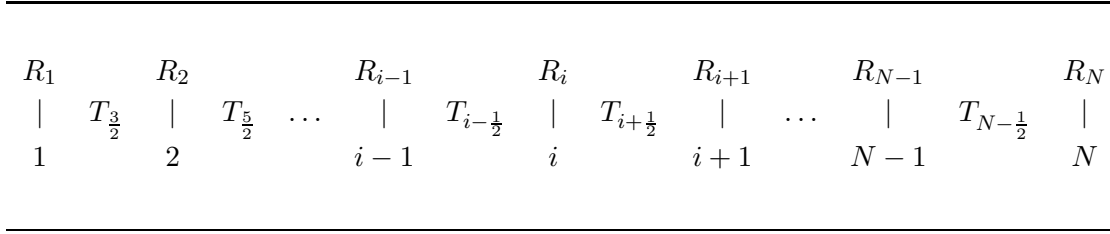


Figure 1. The numerical scheme

$$y^{n+\frac{1}{2}} = \theta_y y^{n+1} + (1 - \theta_y) y^n \quad (7)$$

The superscript $(n + \frac{1}{2})$ on a function of independent variables, *e.g.* the area $A^{n+\frac{1}{2}}$, thus denotes the temporal average of the function. Spatial differences are defined by $\Delta y_i = y_{i+\frac{1}{2}} - y_{i-\frac{1}{2}}$ and $\Delta y_{i+\frac{1}{2}} = y_{i+1} - y_i$, respectively.

Our 3rd equation is for the *total energy* (*i.e.* the sum of the internal, gravitational and kinetic energies) rather than for the *internal energy* alone as in Fraley's scheme. However, Fraley's scheme is such as to actually conserve the global total energy exactly. Therefore our differencing reduces to Fraley's, to within numerical round-off errors when the grid motion is Lagrangean ($u_{rel} = 0$).

2.1. CONTINUITY EQUATION

With the usual definitions

$$V_i^n = \frac{4\pi}{3} (R_i^n)^3 \quad \Delta V_{i+\frac{1}{2}}^n = V_{i+1}^n - V_i^n$$

$$A_i^n = 4\pi (R_i^n)^2 \quad DM_{i+\frac{1}{2}}^n = \rho_{i+\frac{1}{2}}^n \Delta V_{i+\frac{1}{2}}^n$$

the continuity equation takes on the form

$$DM_{i+\frac{1}{2}}^{n+1} - DM_{i+\frac{1}{2}}^n + F_{M,i+1}^{n+\frac{1}{2}} - F_{M,i}^{n+\frac{1}{2}} = 0, \quad (8)$$

where $F_{M,i}^{n+\frac{1}{2}}$ is the mass flux through the zone boundary during the timestep δt .

There are many different ways of specifying the flux. We have chosen the second order scheme of van Leer (1979) for our code. (We have not

experimented with higher schemes, *e.g.* PPM; such schemes are much more cumbersome and expensive to implement, but are not expected to increase the accuracy in the shocks and ionization fronts which are already well resolved, although they might increase the accuracy elsewhere). In the following, the donor cell scheme is used only for the purposes of comparison.

$$\delta t (\rho u_{rel} A)_i^{n+\frac{1}{2}} = F_{M,i}^{n+\frac{1}{2}} = \delta t A_i^{n+\frac{1}{2}} \langle \rho_i^{n+\frac{1}{2}} \rangle u_{rel,i}^{n+\frac{1}{2}} \quad (9)$$

$$\delta t u_{rel,i}^{n+\frac{1}{2}} = \delta t u_i^{n+\frac{1}{2}} - (R_i^{n+1} - R_i^n) \quad (10)$$

$$\langle \rho_i^{n+\frac{1}{2}} \rangle = \mathcal{S}^-(u_{rel,i}) (\rho_{i+\frac{1}{2}}^{n+\frac{1}{2}} + d\rho_{i+\frac{1}{2}}^{n+\frac{1}{2}}) + \mathcal{S}^+(u_{rel,i}) (\rho_{i-\frac{1}{2}}^{n+\frac{1}{2}} - d\rho_{i-\frac{1}{2}}^{n+\frac{1}{2}}) \quad (11)$$

with the switch \mathcal{S} and $d\rho$ are defined as

$$\mathcal{S}^\pm(u) = \frac{1}{2}(1 \pm \text{sgn}(u)) \quad (12)$$

$$d\rho_{i+\frac{1}{2}} = \frac{\Delta\rho_{i+1}\Delta\rho_i}{\rho_{i+\frac{3}{2}} - \rho_{i-\frac{1}{2}}} \mathcal{S}^+(\Delta\rho_{i+1}\Delta\rho_i). \quad (13)$$

For the purpose of comparison only we also use the less accurate first order upwind scheme (donor cell):

$$\langle \rho_i^{n+\frac{1}{2}} \rangle = \mathcal{S}^-(u_{rel,i}) \rho_{i+\frac{1}{2}}^{n+\frac{1}{2}} + \mathcal{S}^+(u_{rel,i}) \rho_{i-\frac{1}{2}}^{n+\frac{1}{2}} \quad (14)$$

2.2. MOMENTUM EQUATION

Again with the usual definition

$$DM_i = \frac{1}{2} \left(DM_{i+\frac{1}{2}} + DM_{i-\frac{1}{2}} \right) \quad (15)$$

the two momentum source terms are differenced as

$$\mathcal{M}_P = \delta t (A\Delta p)_i = \delta t \langle A_i \rangle^{n+\frac{1}{2}} \left(p_{i+\frac{1}{2}}^{n+\frac{1}{2}} - p_{i-\frac{1}{2}}^{n+\frac{1}{2}} \right) \quad (16)$$

$$\mathcal{M}_G = \delta t \left(\frac{GM}{r^2} \rho \Delta V \right)_i = \delta t G \langle \frac{1}{R_i^2} \rangle M_i^{n+\frac{1}{2}} DM_i^{n+\frac{1}{2}} \quad (17)$$

In the Fraley scheme global energy conservation is possible through the introduction of special averages. We therefore introduce the same averages in order to preserve this conservation in the Lagrangean limit

$$\langle A_i \rangle^{n+\frac{1}{2}} = \frac{4\pi}{3} \left((R_i^n)^2 + R_i^{n+1} R_i^n + (R_i^{n+1})^2 \right) \quad (18)$$

$$\left\langle \frac{1}{R_i^2} \right\rangle = \frac{1}{R_i^{n+1} R_i^n} \quad (19)$$

For the fluxes we again use van Leer's expressions

$$\delta t(\rho u u_{rel} A)_i^{n+\frac{1}{2}} \equiv F_{I,i+\frac{1}{2}}^{n+\frac{1}{2}} = \delta t \langle u_{i+\frac{1}{2}}^{n+\frac{1}{2}} \rangle \delta M_{i+\frac{1}{2}} \quad (20)$$

with

$$\langle u_{i+\frac{1}{2}}^{n+\frac{1}{2}} \rangle = \mathcal{S}^-(\delta M_{i+\frac{1}{2}}^{n+\frac{1}{2}})(u_{i+1}^{n+\frac{1}{2}} + du_{i+1}^{n+\frac{1}{2}}) + \mathcal{S}^+(\delta M_{i+\frac{1}{2}}^{n+\frac{1}{2}})(u_i^{n+\frac{1}{2}} - du_i^{n+\frac{1}{2}}) \quad (21)$$

$$du_i = \frac{\Delta u_{i+\frac{1}{2}} \Delta u_{i-\frac{1}{2}}}{u_{i+1} - u_{i-1}} \mathcal{S}^+(\Delta u_{i+\frac{1}{2}} \Delta u_{i-\frac{1}{2}}) \quad (22)$$

$$\delta M_{i+\frac{1}{2}} = \frac{1}{2}(\delta M_{i+1} + \delta M_i). \quad (23)$$

Finally the momentum equation becomes

$$u_i^{n+1} DM_i^{n+1} - u_i^n DM_i^n + \left(F_{I,i+\frac{1}{2}}^{n+\frac{1}{2}} - F_{I,i-\frac{1}{2}}^{n+\frac{1}{2}} \right) + \mathcal{M}_P + \mathcal{M}_G = 0 \quad (24)$$

There are different ways of introducing δM_i . Algebraically it is equal to $F_{M,i}^{n+\frac{1}{2}}$, but numerically this form can cause problems (*cf.* comments by Winkler & Norman 1986, §V.B. on the use of δM). The direct replacement of δM_i by the mass flux also widens the band matrix in the iteration for each timestep as Eqs. 23 and 29 show. Both problems are avoided with the introduction of M_i as an independent variable and its definition

$$\Delta M_{i+\frac{1}{2}} = \rho_{i+\frac{1}{2}} \Delta V_{i+\frac{1}{2}} \quad (25)$$

$$\delta M_i^{n+\frac{1}{2}} = M_i^{n+1} - M_i^n \quad (26)$$

2.3. TOTAL ENERGY EQUATION

A small complication arises because in Fraley's staggered scheme the internal energies are most naturally defined in the cell centers, but the kinetic and gravitational energies are defined at the cell boundaries. We therefore define the cell's total energy as being its internal energy plus one half of the combined kinetic and gravitational energies of its edges.

$$E_{i+\frac{1}{2}} = e_{i+\frac{1}{2}} DM_{i+\frac{1}{2}} + g_{i+1} DM_{i+1} + g_i DM_i \quad (27)$$

$$g_i = \frac{1}{2} \left(\frac{(u_i)^2}{2} - \frac{GM_i}{R_i} \right) \quad (28)$$

In accordance with Fraley's scheme we define the 'pressure-work'

$$(puA)_i^{n+\frac{1}{2}} = \langle A_i^{n+\frac{1}{2}} \rangle u_i^{n+\frac{1}{2}} \frac{1}{2} \left(p_{i+\frac{1}{2}}^{n+\frac{1}{2}} + p_{i-\frac{1}{2}}^{n+\frac{1}{2}} \right) \quad (29)$$

The total energy equation is

$$(E_{i+\frac{1}{2}}^{n+1} - E_{i+\frac{1}{2}}^n) + \delta t \left(L_{i+1} - L_i + (puA)_{i+1} - (puA)_i \right)^{n+\frac{1}{2}} + (F_{Ei+1}^{n+\frac{1}{2}} - F_{Ei}^{n+\frac{1}{2}}) = 0 \quad (30)$$

Note that the equation is written in full conservation form as a set of spatial differences, Δ . We define the relative energy flux again in the van Leer's fashion. Care has to be taken to center the corresponding fluxes correctly *i.e.* consistently with Eq. 27. First we calculate the advection terms of the kinetic energy at the cell centers, then calculate the spatial average at the cell boundaries where the internal energy flux is naturally defined. Other kinds of averaging, such as first calculating the the total energy density at cell centers and then advecting this quantity by $\delta M_i^{n+\frac{1}{2}}$, can lead to numerical instabilities.

$$F_{Ei}^{n+\frac{1}{2}} = \delta t \left[\langle e_i^{n+\frac{1}{2}} \rangle \delta M_i^{n+\frac{1}{2}} + \langle g_{i-\frac{1}{2}}^{n+\frac{1}{2}} \rangle \delta M_{i-\frac{1}{2}}^{n+\frac{1}{2}} + \langle g_{i+\frac{1}{2}}^{n+\frac{1}{2}} \rangle \delta M_{i+\frac{1}{2}}^{n+\frac{1}{2}} \right] \quad (31)$$

$$\langle e_i^{n+\frac{1}{2}} \rangle = \mathcal{S}^- (\delta M_i^{n+\frac{1}{2}}) (e_{i+\frac{1}{2}}^{n+\frac{1}{2}} + de_{i+\frac{1}{2}}^{n+\frac{1}{2}}) + \mathcal{S}^+ (\delta M_i^{n+\frac{1}{2}}) (e_{i+\frac{1}{2}}^{n-\frac{1}{2}} - de_{i-\frac{1}{2}}^{n+\frac{1}{2}}) \quad (32)$$

$$\langle g_{i+\frac{1}{2}}^{n+\frac{1}{2}} \rangle = \mathcal{S}^- (\delta M_{i+\frac{1}{2}}^{n+\frac{1}{2}}) (g_{i+1}^{n+\frac{1}{2}} + dg_{i+1}^{n+\frac{1}{2}}) + \mathcal{S}^+ (\delta M_{i+\frac{1}{2}}^{n+\frac{1}{2}}) (g_i^{n+\frac{1}{2}} - dg_i^{n+\frac{1}{2}}) \quad (33)$$

$$de_{i+\frac{1}{2}} = \frac{\Delta e_{i+1} \Delta e_i}{e_{i+\frac{3}{2}} - e_{i-\frac{1}{2}}} \mathcal{S}^+ (\Delta e_{i+1} \Delta e_i). \quad (34)$$

$$du_i = \frac{\Delta g_{i+\frac{1}{2}} \Delta g_{i-\frac{1}{2}}}{g_{i+1} - g_{i-1}} \mathcal{S}^+ (\Delta g_{i+\frac{1}{2}} \Delta g_{i-\frac{1}{2}}) \quad (35)$$

The luminosity L is taken here in the radiation equilibrium diffusion approximation

$$L = -(4\pi r^2)^2 c \frac{1}{\kappa(\rho, T)} \frac{d}{dm} \frac{aT^4}{3} \quad (36)$$

We generally use the difference form suggested by Stellingwerf (1974) which averages T^4/κ , but keep the option of using Stobie's (1969) average of the opacity.

Finally a word about time-centering. Fraley's scheme is *stable* for $\theta \geq \frac{1}{2}$. It is therefore tempting to increase the stability of the code by making all $\theta > 0.5$. However, in order to globally ensure total energy conservation in the Lagrangean limit, it is necessary to use $\theta_u = \frac{1}{2}$ for

the velocity (Fraley 1968). Furthermore, decentering the pressure in Eqs. (16) and (29) leads to improper mode growth or decay. In fact, it can be shown that even in the adiabatic limit the linear eigenvalues incorrectly become complex (Kovács, private communication); it is therefore important to set $\theta_p = \frac{1}{2}$ as well. Following Stellingwerf and our past experience we use $\theta = \frac{2}{3}$ for the luminous flux L which has a small effect on the global results, except that is numerically stabilizing and reduces jitter. (Aside from the special Fraley averages $\langle A \rangle$ and $\langle 1/R^2 \rangle$ the luminosity L is therefore the only function that is not centered in time).

In some calculations, for test purposes only, we replace the the total energy difference equations (30) by the appropriate internal energy difference equations, *viz.*

$$(U_{i+\frac{1}{2}}^{n+1} - U_{i+\frac{1}{2}}^n) + \delta t \left((L_{i+1}^{n+\frac{1}{2}} - L_i^{n+\frac{1}{2}}) + p_{i+\frac{1}{2}} \Delta(\langle A \rangle u)_{i+\frac{1}{2}} \right) \quad (37)$$

$$(38)$$

$$+ (F_{U_{i+1}}^{n+\frac{1}{2}} - F_{U_i}^{n+\frac{1}{2}}) = 0$$

where the internal energy is $U_{i+\frac{1}{2}} = e_{i+\frac{1}{2}} \Delta M_{i+\frac{1}{2}}$, the internal energy flux $F_{U_i}^{n+\frac{1}{2}} = \delta t \langle e_i^{n+\frac{1}{2}} \rangle \delta M_i^{n+\frac{1}{2}}$ with $\langle e_i^{n+\frac{1}{2}} \rangle$ as defined in Eq. 32.

We note that this internal energy equation is also the equation solved by Gehmeyr and by Dorfi *et al.* (*loc. cit.*). We note in anticipation that the performance of the code greatly deteriorates when this substitution is made.

2.4. PSEUDO-VISCOSITY

Finally a word about pseudo-viscosity. Our pressure everywhere includes a von Neumann–Richtmyer (vNR) viscosity with a Stellingwerf cut-off parameter α_q , involving the local sound velocity c , of the form

$$p_{visc,i+\frac{1}{2}} = C_q \rho_{i+\frac{1}{2}} \left(\left[(u_{i+1} - u_i) - \alpha_q c_{s,i+\frac{1}{2}} \right]_+ \right)^2 \quad (39)$$

In the case where spherical geometric effects are important this expression is advantageously replaced by the form suggested by Whalen (*cf.* Buchler & Whalen 1990, Eqs. 9–10).

It may seem strange to still use pseudo-viscosity when the applied mathematical literature abounds in 'better' ways of treating shocks (*e.g.* Buchler 1990). First, we note that the use of flux limiters and Riemann solvers (*e.g.* Roe in Buchler 1990) assumes that the hydrodynamics equations are written in a very specific 'conservative' form

which is not the case in our scheme, because of our desire to preserve the good features of the Fraley scheme. Eqs. 1–6 show that in a Lagrangean or near Lagrangean situation all but the 'pressure-work' flux and the radiative fluxes disappear and that the code would be unstable in the absence of pseudo-viscosity. Since, during the pulsation, parts of the mesh can indeed behave in a manner close to Lagrangean the possibility of such instability is not desirable. In our 'defense' we also note that when the grid motion redistributes mesh points into the shock, the effects of the pseudo-viscosity are largely reduced.

2.5. THE MESH EQUATION

Within constraints of stability, and ultimately accuracy, the choice of the mesh motion is to a large extent an art. On one extreme are the Eulerian and Lagrangean descriptions with a 'rigid' mesh, with $u_{grid} = \text{constant}$ and $u_{rel} = 0$, respectively, and on the other the mesh motions which follow the dynamics so rapidly and faithfully that the physical quantities are largely constant. A good mesh-function clearly lies in between.

We have had good experience with Lagrangean meshes in which the outer zones, say up to hydrogen ionization ($\approx 11,000$ K) were equally spaced and the mesh size then increased geometrically inward. In the spirit of our conservative approach we therefore want to stay as close as possible to this type of mesh both in the static model and in the hydro-code. We want to use the adaptive features primarily, first, to resolve the partial hydrogen ionization during the pulsation, and second, to resolve shocks better than is possible with a standard Lagrangean mesh.

For these reasons we adopt a mesh density defined in terms of the mass, rather than the radius, *viz.*

$$n_{i+\frac{1}{2}} = \frac{X_{i+\frac{1}{2}}}{\Delta M_{i+\frac{1}{2}}}, \quad (40)$$

but for tests we keep the option of using the radius in the mesh density (*i.e.* $n_{i+\frac{1}{2}} = X_{i+\frac{1}{2}}/\Delta R_{i+\frac{1}{2}}$). The quantity $X_{i+\frac{1}{2}}$ is a mass scale (or length scale). In the case of periodic pulsators our methodology will be to use first the fast Lagrangean Stellingwerf code to obtain the limit cycles and then to switch over to an adaptive mesh with a minimum of transients. For this reason we use the cell masses $\Delta M_{i+\frac{1}{2}}^{(0)}$ of the equilibrium model for the scaling, *viz.* $X_{i+\frac{1}{2}} = \Delta M_{i+\frac{1}{2}}^{(0)}$. This scale $X_{i+\frac{1}{2}}$ is thus held constant during the calculation. With this definition of $X_{i+\frac{1}{2}}$ the grid density is uniformly equal to 1 in the equilibrium model and in the Lagrangean code. We note that in general the magnitude of

$n_{i+\frac{1}{2}}$ depends on the definition of $X_{i+\frac{1}{2}}$ and really has a meaning only relative to the values of the grid density at different zones; in other words, generally the value of the grid density has nothing to do with the grid resolution.

Otherwise we adopt the mesh diffusion (parameter α) and relaxation time (τ) of Dorfi & Drury (1987):

$$\hat{n}_{i+\frac{1}{2}} = n_{i+\frac{1}{2}} - \alpha(1 - \alpha)(n_{i+\frac{3}{2}} - 2n_{i+\frac{1}{2}} + n_{i-\frac{1}{2}}) \quad (41)$$

$$\tilde{n}_{i+\frac{1}{2}}^{n+1} = \hat{n}_{i+\frac{1}{2}}^{n+1} + \frac{\tau}{\delta t}(\hat{n}_{i+\frac{1}{2}}^{n+1} - \hat{n}_{i+\frac{1}{2}}^n) \quad (42)$$

For the structure function which gives the necessary grid resolution we have found it convenient to use the following function:

$$Z_{i+\frac{1}{2}} = \left(1 + \sum_k \beta_k S_{i+\frac{1}{2}} \left(\frac{\Delta f_{i+\frac{1}{2}}^{(k)}}{F_{i+\frac{1}{2}}^{(k)}} \right)^2 \right)^{1/2}, \quad (43)$$

where the scale factor

$$S_{i+\frac{1}{2}} = \frac{n_{i+\frac{1}{2}}}{1 + (s n_{i+\frac{1}{2}})^4} \quad (44)$$

is introduced to give an upper limit to the grid density, *viz.* $1/s$. Without the fourth order term in the denominator the grid density could increase unlimitedly causing numerical problems at velocity discontinuities: The artificial viscosity (Eq. 38) puts a constant number of grid points in the shock region, a number that is governed by the parameter C_q . This leads to constant velocity difference Δu independently of the current grid density. If then the $\Delta f_{i+\frac{1}{2}}^{(k)}/F_{i+\frac{1}{2}}^{(k)}$ term in Eq. 42 is dominated by Δu , the larger value of grid density generates a larger value of $Z_{i+\frac{1}{2}}$ and causes another increase of n . This positive feedback is stopped by the upper limit of grid density.

Generally we introduce two terms in the sum (42), *viz.*

$$\Delta f_{i+\frac{1}{2}}^{(1)} = T_{i+\frac{3}{2}} - T_{i-\frac{1}{2}}, \quad F_{i+\frac{1}{2}}^{(1)} = T_{i+\frac{1}{2}} \quad (45)$$

$$\Delta f_{i+\frac{1}{2}}^{(2)} = u_{i+1} - u_i, \quad F_{i+\frac{1}{2}}^{(2)} = u_o \quad (46)$$

Here the quantity u_o represents the velocity scale of the problem which can be mesh and time dependent. The $f^{(1)}$ function serves the purpose of placing meshpoints in the regions of rapidly varying temperature, such as in the partial hydrogen ionization region which has a very sharp temperature variation, particularly in classical Cepheids. The

$f^{(2)}$ function acts only when strong velocity gradients are present and its obvious purpose is to resolve shocks.

With these preambles the mesh equation finally is

$$\frac{\tilde{n}_{i+\frac{1}{2}}}{Z_{i+\frac{1}{2}}} = \frac{\tilde{n}_{i-\frac{1}{2}}}{Z_{i-\frac{1}{2}}} \quad (47)$$

The specification of our mesh function is incomplete without boundary conditions. First we impose that the mesh be Lagrangean in the first few inner zones and in the last few zones. Second, following Dorfi & Drury (1987) we impose that $n_{i-\frac{1}{2}} = n_{i+\frac{1}{2}}$ at both Lagrange-adaptive interfaces.

With our definition of the grid density ($n_{i+\frac{1}{2}} = \Delta M_{i+\frac{1}{2}}^{(0)} / \Delta M_{i+\frac{1}{2}}$) the grid motion is Lagrangean when $\beta_k = 0$ because $Z_{i+\frac{1}{2}} = 1$ and $\Delta M_{i+\frac{1}{2}}$ remains constant. In other words the mesh equation is always satisfied when the β_k parameters are set to zero and the mass distribution is given by the initial Lagrangean model ($Z_{i+\frac{1}{2}} = n_{i+\frac{1}{2}} = 1$). By a gradual increase of the β_k it is possible to evolve the Lagrange grid into the adaptive one (*cf.* also §3.3).

For test purposes we have also experimented with the radius differences in the grid density with $X_{i+\frac{1}{2}} = \Delta R_{i+\frac{1}{2}}^{in}$ (*i.e.* $n_{i+\frac{1}{2}} = \Delta R_{i+\frac{1}{2}}^{in} / \Delta R_{i+\frac{1}{2}}$). In that case the $\beta_k = 0$ condition gives a simplified grid equation: $\Delta R_{i+\frac{1}{2}} / \Delta R_{i-\frac{1}{2}} = \text{constant}$, which defines a *quasi Eulerian* grid motion. Since several zones at the top and the bottom of the model are Lagrangean, the grid motion of these special zones are given by the fluid motion: $R_{gr,L}^n = R_L^n$. With these boundary conditions the solution of the simplified grid equation becomes

$$R_i^n = R_{L_1}^n + \frac{R_i^0 - R_{L_2}^0}{R_{L_2}^0 - R_{L_1}^0} (R_{L_2}^n - R_{L_1}^n), \quad (48)$$

where R_{L_1} and R_{L_2} are the radius variations of the two Lagrangean zones bracketing the quasi Eulerian grid.

3. Tests

As performance tests for the code we have chosen the challenging Noh spherical shock problem (Noh 1987) and Sedov's (1959) point explosion problem. Analytical solutions exist in both cases. A perfect gas equation of state with ($\gamma = 5/3$) has been used for these tests. We will also present calculations for Cepheid model pulsations with a realistic equation of state and opacities to show the application of the code to stellar oscillations.

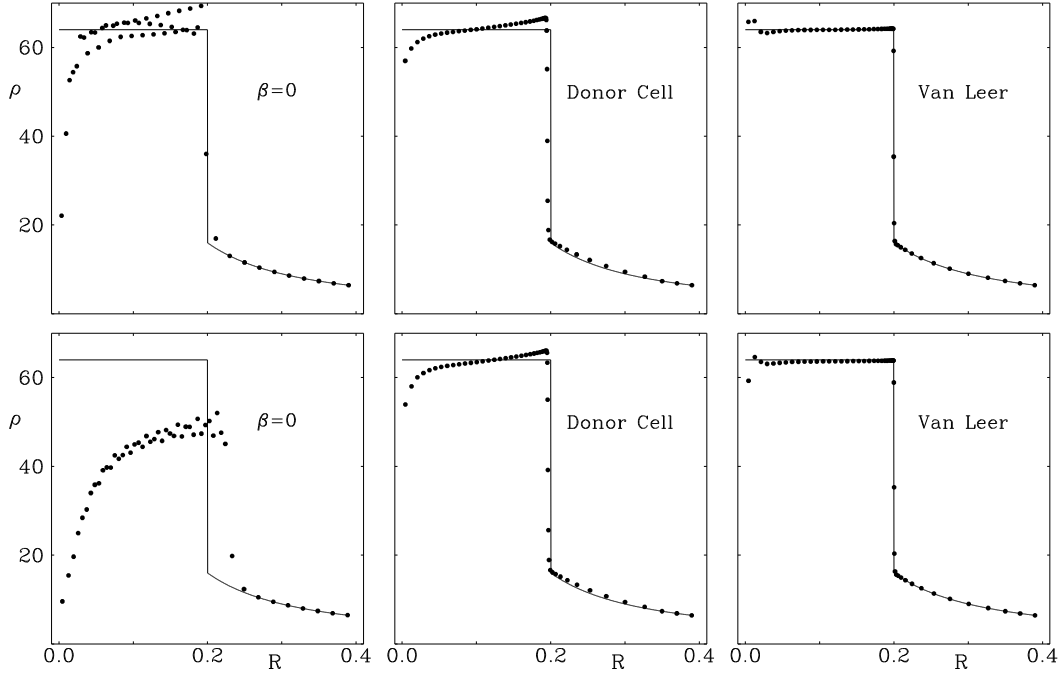


Figure 2. Numerical solution of the spherical Noh problem at $t=0.6$. Upper panels: tensor viscosity, lower panels: vNR viscosity, ΔM is used in the mesh density.

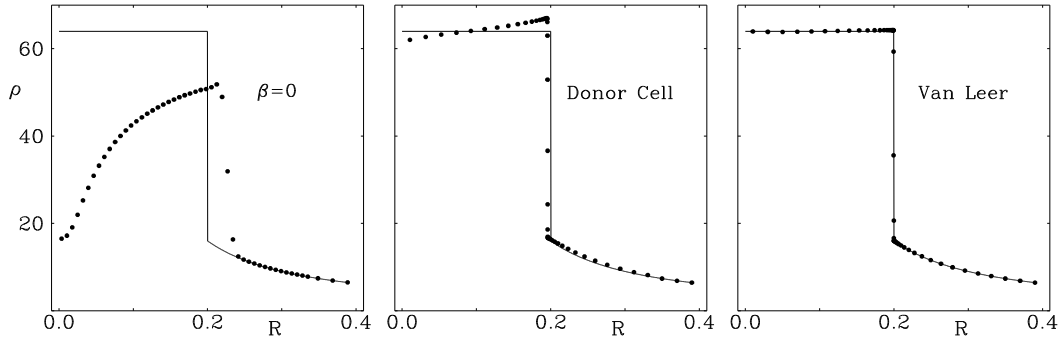


Figure 3. Spherical Noh problem. ΔR is used in the grid density; vNR viscosity.

3.1. SPHERICAL NOH PROBLEM

The initial conditions for the Noh problem are uniform velocity ($u_j = -1$) and density ($\rho_j = 1$) with zero pressure and temperature. The shock generated at the center of the sphere moves outward with a constant speed ($v = 1/3$). The density has a flat profile behind the shock with $\rho = 64$ at all times.

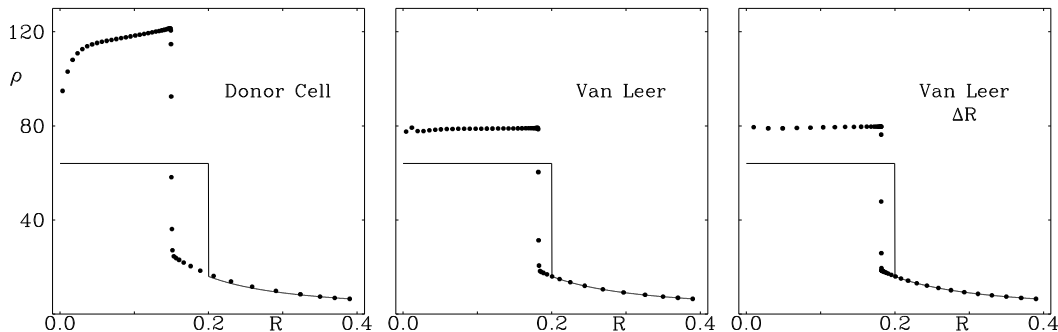


Figure 4. Spherical Noh problem. The internal energy eq. is solved instead of the total energy eq.; vNR viscosity

For the numerical solution we have used a mesh with 50 zones initially spaced with equal ΔR . Since the spherical geometric effects are important we have also used the tensor artificial viscosity for these calculations (For a comparison of different treatments of artificial viscosity in Lagrangean calculations see Buchler and Whalen 1990). The parameters of the calculations are the following: $C_q=1.0$, $\beta_u = 1000$, $s=0.0002$, $\tau=0.0005$, $\alpha=2.0$ and $u_o = 1$.

Figure 2. displays the results of the calculations for different parameters together with the analytic solution. For the upper and lower row the Whalen tensor and the von Neumann-Richtmyer viscosity have been used, respectively. The adaptive calculation with the first order upwind scheme (second column) considerably improves the solution over the Lagrangean limit ($\beta_u=0$) which exhibits unphysical oscillations behind the shock. The use of the van Leer advection provides superior results (third column). This test clearly demonstrates that the higher order advection scheme is preferable in the adaptive calculation. The results are independent of the choice of the artificial viscosity, in fact the use of the tensor artificial viscosity is not necessary with the adaptive computation even in this problem with strong sphericity.

In Fig. 3. we present the solutions with an alternate form for the grid density, *viz.* with $\Delta R_{i+\frac{1}{2}}$ in the denominator in Eq. 39. The vNR artificial viscosity is used. The first panel shows the quasi Eulerian result ($\beta_u=0$). The result with $\Delta R_{i+\frac{1}{2}}$ is a little better than the one with $\Delta M_{i+\frac{1}{2}}$, especially at the center, but the difference is insignificant elsewhere. (The glitch near the center is due to the inaccuracies introduced by the steeply varying cell mass in the initial profile which has been constructed with equal ΔR .)

We have to emphasize that solving the *total energy equation* (Eq. 30) has been crucial in getting a correct solution for the Noh problem. We

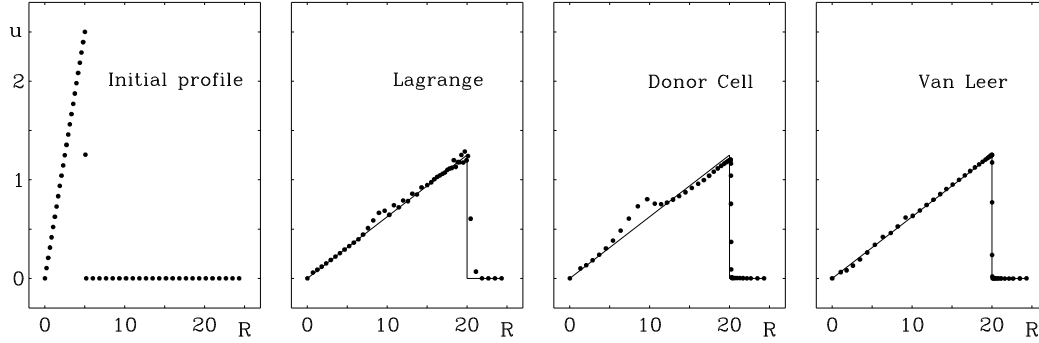


Figure 5. Numerical solution of the Sedov problem. From left to right: initial velocity profile, Lagrangean and adaptive results.

illustrate this in Figure 4 which shows the results for a calculation in which we now solve the internal energy equation (Eq. 437). It is true that with the adaptive mesh code we still get a sharp shock, but the velocity of the shock front (and thus the density) is very different from the correct values. When we monitor the time-dependence of the energies we notice a small gradual decrease in the global total energy (4.2% at $t=0.6$). Furthermore, the kinetic energy is too large and correspondingly the internal too small by $\approx 7.3\%$ and 15.6% respectively, whereas with the solution of the total energy equation the discrepancy in kinetic energy is less than 0.5%, *i.e.* 10 times less. In the Lagrangean limit, of course, the two energy equations yield the same solution to machine accuracy (because of the already mentioned property of the Fraley scheme).

The order of the advection scheme plays a much more important role in the accuracy of the calculations when the internal energy equation is solved, as a comparison of Fig. 2 (top middle and top right) and Fig. 4 (left and middle) shows. This is an indication that the advection errors are much larger for the internal energy equation. An additional reason for the inaccuracies is found in the differencing of the source term (Eq. 37) $p\Delta(\langle A \rangle u)$ which can vary very rapidly throughout the shock. In contrast, the total energy equation contains only flux terms and the corresponding Hugoniot–Rankine equation is automatically satisfied through near-discontinuities.

The middle and right graphs of Figure 4 show that the inaccuracies associated with the solution of the internal energy equation occur for both definitions of mesh density (mass *vs.* radius).

3.2. SEDOV PROBLEM

The analytic solution of an intense point explosion in a power-law density gradient with spherical symmetry is given by Sedov (1959). The motion of the gas is self-similar *i.e.* the shapes of the pressure, density and velocity profiles remain the same during the explosion. For an ideal gas with $\gamma = 5/3$ the distance of the shock front from the center (R_s) is proportional to $t^{2/3}$, and the physical parameters behind the shock are given by the initial value of the pressure, density and shock velocity. For an initial density given by $\rho(R) = AR^{-2}$ the solution has the form

$$u = \frac{R}{2t} \quad \rho = \frac{4AR}{R_s^3} \quad p = \frac{A}{3t^2} \left(\frac{R}{R_s} \right)^3, \quad (49)$$

for radii R less than the radial distance of the shock (R_s). The energy of the explosion appears in these functions only through the location of the shock front (R_s) for a given time.

We choose the explosion energy so that the position of the shock at $t=1$ is $R_s=5$ (in arbitrary units). Our initial model is constructed by discretizing the exact solution for $t=1$. Half of the 50 zones are placed below the front. The zones are initially equally spaced in ΔR , but with different spacings below and above the front to get approximately the same zone mass on both sides. We use ΔM in the grid density. The numerical parameters are $C_q=1.0$, $\beta_u = 1000$, $s=0.005$, $\tau=0.003$, $\alpha=2.0$ and $u_o = 1$.

The Lagrangean and adaptive solutions at $t=8$ are shown in Figure 5 for the van Leer scheme. For comparison only Donor Cell results are also shown. By this time the intense shock, with density ratio 4:1 across the front, has progressed to a density 1/16 times the density at the start of the calculation.

When the initial grid distribution does not satisfy the mesh equation, which is the general situation, transient oscillations appear in the solution. Figure 5 shows that the initial transient leaves a large incorrect permanent scar on the solution when the inaccurate donor cell advection scheme is used. Only when we use the second order scheme are the fluctuations in the velocity minimal, and the position of the shock front is correctly obtained.

As for the Noh problem, we again find it important to solve the total energy equation rather than the internal energy equation. With the use of the internal energy equation, the resulting shock is still sharp, but it lags. For example, at $t=8$ the position of the front is $R_s=19.4$ instead of the correct value of $R_s=20$. The accumulated error in the total energy reaches 10% for this time. The total kinetic energy which should be

constant during the shock propagation is also decreasing at the same rate. It is this underestimation of the kinetic energy that causes the error in the shock position.

3.3. CEPHEID PULSATIONS

Table I. Typical errors of the total energy – Cepheid model problem.

| j_L | $T(j_L)$ [K] | $\epsilon_A(E_{tot})$ | $\epsilon(E_{tot})/P$ | Scheme |
|-------|----------------|-----------------------|-----------------------|------------|
| 60 | $5 \cdot 10^4$ | $4.0 \cdot 10^{-9}$ | $-1.0 \cdot 10^{-9}$ | van Leer |
| 40 | $1 \cdot 10^5$ | $1.5 \cdot 10^{-7}$ | $-1.5 \cdot 10^{-8}$ | van Leer |
| 30 | $2 \cdot 10^5$ | $4.0 \cdot 10^{-7}$ | $+1.0 \cdot 10^{-8}$ | van Leer |
| 60 | $5 \cdot 10^4$ | $3.0 \cdot 10^{-8}$ | $-6.0 \cdot 10^{-8}$ | Donor Cell |
| 40 | $1 \cdot 10^5$ | $4.0 \cdot 10^{-6}$ | $-5.0 \cdot 10^{-6}$ | Donor Cell |

We have selected a model from one of the Cepheid sequences of Moskalik, Buchler and Marom (1992). We use the OPAL opacities (Iglesias *et al.* 1992) matched with the opacities of Alexander and Ferguson (1994) at low temperatures. The chemical composition is $X=0.7$, $Z=0.02$. The computations are performed with 120 mass zones. The static model has been built as follows: equal mass zones inward from the surface; a temperature anchor of 11,000K in the 30th inward zone; the mass of the inner zones increases geometrically up to an inner temperature of $T_{in} = 2 \times 10^6$ K (This is the same type of grid that has been found to give good results in the Lagrangean code, *e.g.* Moskalik *et al.* 1992). This mass distribution also gives the reference grid for the adaptive calculations by setting the values of $X_{i+\frac{1}{2}}$, as discussed earlier. With the stellar parameters $M=6.5M_\odot$, $L=7213L_\odot$ and $T_{eff}=5404$ K the period of the model is ≈ 18 days.

It is notoriously difficult to get rid of long lasting transient oscillations in an adaptive code. We have found the following procedure to be very useful in the case of periodic pulsations (asymptotic limit cycle). A limit cycle solution is first calculated with the relaxation method of Stellingwerf applied to the Lagrangean code (starting from a perturbed static equilibrium model). This pulsating model is then inserted into the adaptive code in its Lagrangean mode, and the adaptive mesh is gradually switched on. More specifically, the β_k parameters of the structure function are increased during the first s periods according to

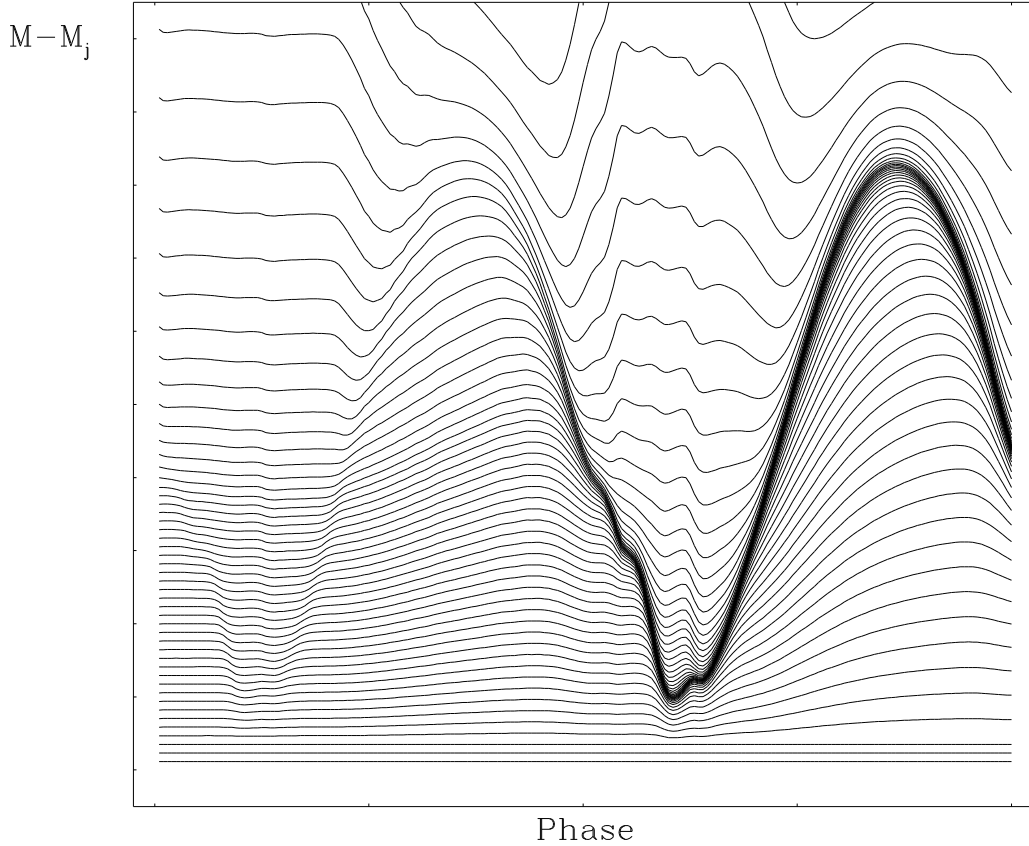


Figure 6. Transition from Lagrange to adaptive grid.

the following recipe:

$$\beta_k = 10^{3t/sP-3} \beta_k^0, \quad (50)$$

and they are then held constant for $t > sP$. This smooth switching on of the grid parameters transforms the Lagrangean mesh into an adaptive one. Since the grid equation is satisfied at the beginning of the calculation (*i.e.* in the $\beta_k=0$, Lagrangean limit) we can evolve the model from Lagrangean to adaptive smoothly by this method and avoid annoying and often very slowly decaying transients. When the advection errors are small (see below) the code converges from a Lagrangean to an adaptive grid limit cycle in several tens of periods.

The transition of the grid from Lagrangean to adaptive is shown in Figure 6 for $s = 2$. The positions of the zones are given by $M - M_j$ ($j=70-120$). The location of the partial ionization region is clearly revealed by the higher grid density which it attracts during the second period of pulsation.

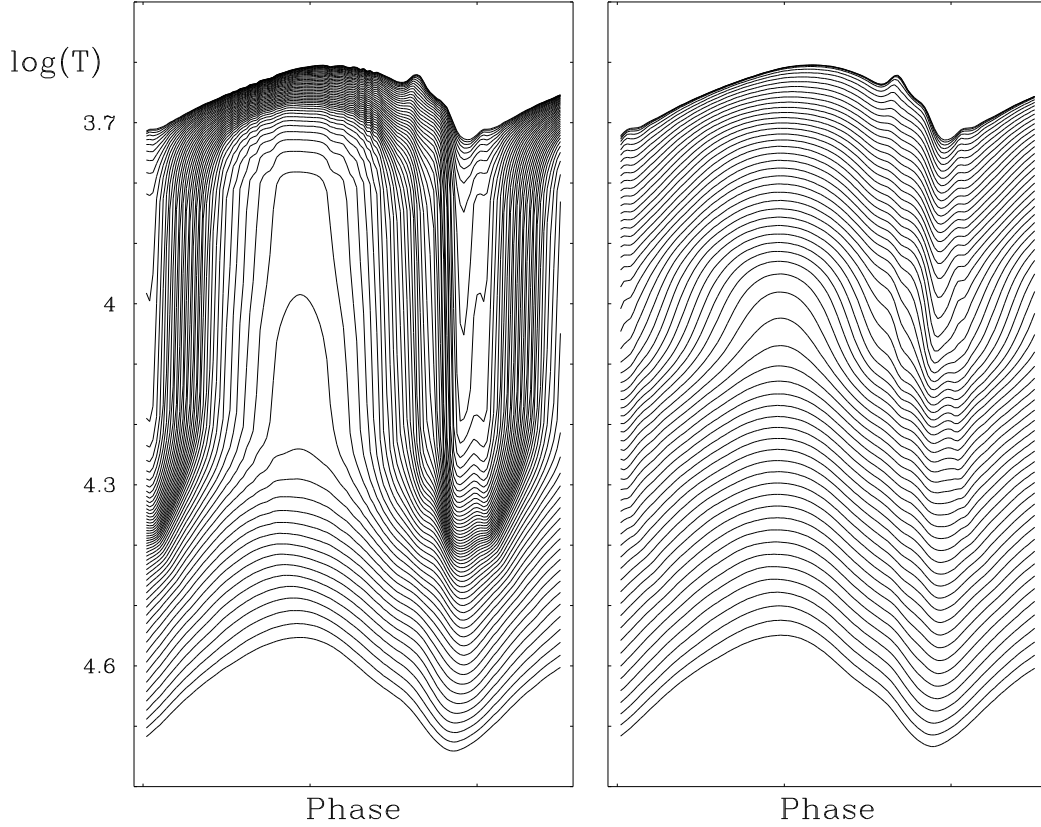


Figure 7. Temperature profiles for the bump-Cepheid model Left box: Lagrangean grid, right box: adaptive grid

The temperature parameter of the structure function is set to $\beta_T^o = 100$. For most of the tests we have used $\beta_u^o = 0$ (the resolution in temperature is enough to get a smooth variation), but we also have made calculations with $\beta_u^o = 10$ and $u_o = 10^5 \text{cm/s}$. This results in a sharper shocks, but too large a value of β_u^o attracts too many points into the shock and away from the partial ionization front, so that the latter loses its sharpness. The given values represent a good compromise between the two tendencies for this number (120) of total mesh points. For the other parameters we have chosen the values $s=0.005$, $\tau=0.1$ days and $\alpha=2.0$. The pseudo viscosity in the form of Eq. 43 is used with $C_q=4$ (for some tests $C_q=1$) and $\alpha_q=0.01$.

The spatial switch-over from Lagrangean to adaptive mesh occurs at zone j_L . When it is made too far inside the stellar model (small j_L) we experience a numerical instability. This happens whether we solve the total energy equation or the internal energy equation. We note that

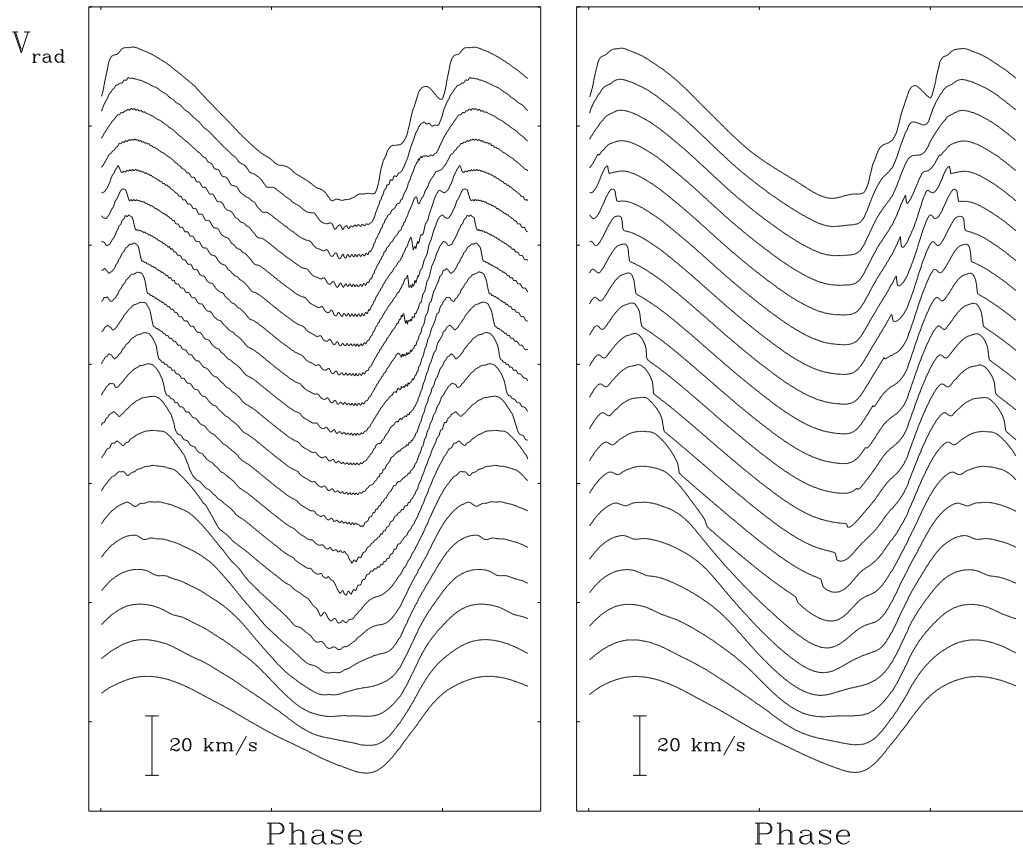


Figure 8. Velocity profiles for the bump-Cepheid model. Left: Langrangean, right: adaptive grid.

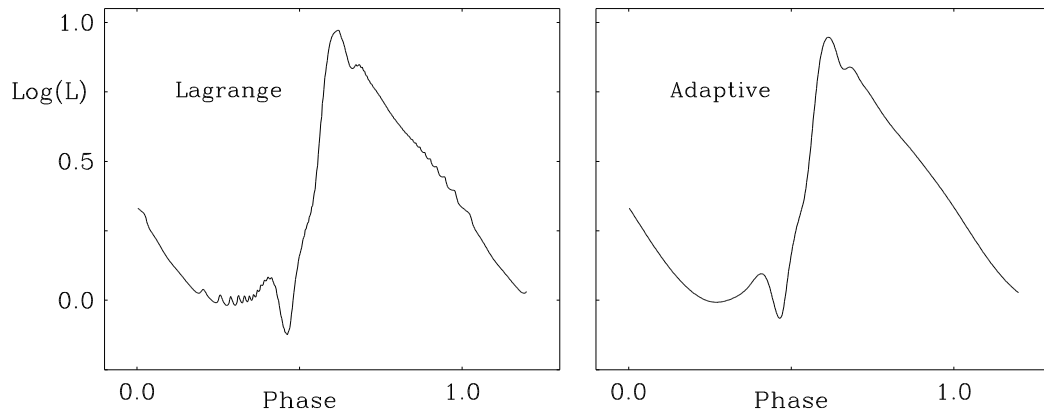


Figure 9. Light-curve. Left: Langrangean, right: adaptive grid.

Table II. Fourier parameters of the limit cycle solution – radius variation. (LA: Lagrangean; TE: total energy, IE internal energy Eqs. are solved; vL: van Leer, DC: donor cell.

| j_L | C_q | | Scheme | P_0 | A_1 | R_{21} | R_{31} | ϕ_{21} | ϕ_{31} |
|-------|-------|----|--------|-------|-------|----------|----------|-------------|-------------|
| – | 4 | LA | – | 17.6 | 22.6 | 0.193 | 0.017 | 6.159 | 0.725 |
| – | 1 | LA | – | 17.6 | 23.2 | 0.197 | 0.021 | 6.176 | 0.906 |
| 60 | 4 | TE | vL | 17.6 | 22.5 | 0.197 | 0.026 | 6.190 | 0.534 |
| 60 | 4 | IE | vL | 17.6 | 22.5 | 0.195 | 0.025 | 6.194 | 0.569 |
| 60 | 1 | TE | vL | 17.6 | 23.1 | 0.199 | 0.027 | 6.200 | 0.824 |
| 60 | 1 | IE | vL | 17.6 | 23.1 | 0.199 | 0.027 | 6.203 | 0.842 |
| 40 | 4 | TE | vL | 17.5 | 22.1 | 0.186 | 0.024 | 6.213 | 0.590 |
| 40 | 4 | IE | vL | 17.5 | 21.3 | 0.182 | 0.017 | 6.177 | 0.307 |
| 40 | 4 | TE | DC | 18.7 | 35.4 | 0.347 | 0.159 | 6.265 | 6.121 |
| 40 | 4 | IE | DC | 18.0 | 17.0 | 0.148 | 0.070 | 0.395 | 1.176 |
| 30 | 4 | TE | vL | 17.3 | 17.5 | 0.138 | 0.033 | 0.127 | 1.207 |
| 30 | 4 | IE | vL | 17.3 | 16.6 | 0.130 | 0.018 | 0.021 | 1.185 |

the same problem has been encountered by Feuchtinger & Dorfi (1994). The reason ultimately lies in the mesh equation. The global nature of the mesh equation and the mesh motions that occur in the outer zones because of moving physical features (mostly the H ionization front) induce small mesh motions even in the relatively quiescent inner zones. However, because of the large masses of these zones the internal and total energy advection errors can therefore reach the order of the small pulsation energy itself. The indication that the trouble is caused by advection errors can be glimpsed from Table 1. Here we report results obtained with the use of the internal energy equation (Eq. 37) because this lets us then monitor total energy conservation. We show both the long-term global error $\epsilon(E_{tot})$, defined as the sum of the errors per cycle of all the zones divided by E_{tot} , and the amplitude of the error fluctuations during the cycle $\epsilon_A(E_{tot})$ (also normalized by E_{tot}). (All the errors are below the convergence parameter, 10^{-5} , of the internal iterations of the code.) The long term error is indeed seen to be substantially larger with the first order advection scheme. When the first order scheme is used, the variation of the energy error is dominated by the long term trend.

Table III. Fourier parameters of the limit cycle solution – magnitude variation. (LA: Lagrangean; TE: total energy, IE internal energy Eqs. are solved; vL: van Leer, DC: donor cell.

| j_L | C_q | | Scheme | P_0 | A_1 | R_{21} | R_{31} | ϕ_{21} | ϕ_{31} |
|-------|-------|----|--------|-------|-------|----------|----------|-------------|-------------|
| – | 4 | LA | – | 17.6 | 0.41 | 0.307 | 0.250 | 5.815 | 5.324 |
| – | 1 | LA | – | 17.6 | 0.42 | 0.310 | 0.250 | 5.837 | 5.328 |
| 60 | 4 | TE | vL | 17.6 | 0.41 | 0.299 | 0.229 | 5.817 | 5.202 |
| 60 | 4 | IE | vL | 17.6 | 0.41 | 0.300 | 0.229 | 5.825 | 5.212 |
| 60 | 1 | TE | vL | 17.6 | 0.42 | 0.301 | 0.248 | 5.784 | 5.226 |
| 60 | 1 | IE | vL | 17.6 | 0.42 | 0.301 | 0.249 | 5.790 | 5.227 |
| 40 | 4 | TE | vL | 17.5 | 0.40 | 0.276 | 0.211 | 5.878 | 5.089 |
| 40 | 4 | IE | vL | 17.5 | 0.38 | 0.282 | 0.209 | 5.851 | 5.162 |
| 40 | 4 | TE | DC | 18.7 | 0.64 | 0.364 | 0.144 | 0.049 | 6.082 |
| 40 | 4 | IE | DC | 18.0 | 0.31 | 0.209 | 0.171 | 5.712 | 4.461 |
| 30 | 4 | TE | vL | 17.3 | 0.32 | 0.241 | 0.151 | 5.792 | 4.861 |
| 30 | 4 | IE | vL | 17.3 | 0.30 | 0.248 | 0.143 | 5.778 | 4.990 |

The solution to the numerical instability is to make the motion of the inner envelope Lagrangean, as Feuchtinger & Dorfi (1994) have also found. The selection of the location of the switching point j_L between adaptive and Lagrangean mesh is important, though, as Table 1 shows. An optimal switch j_L should be as far out in the envelope as possible, but above the He II ionization (at $T > 5 - 10 \times 10^4$ K).

Unfortunately no suitable analytical results exist for a stellar pulsator model against which one could check the codes. We therefore have to rely on the robustness of the results with respect to numerical parameters on the one hand, and to the agreement that we can achieve with the observational data. Although it is important that the pulsations should exhibit long term stability (total energy and pulsation energies constant), this, by itself, is not a guarantee that the amplitude of the cycle is in fact correct.

In order to compare the robustness of the computed limit cycle pulsation we display their Fourier parameters, for the radial velocity of the photo-sphere in Table II and for the stellar magnitude in Table III.

First we note that the calculations with the new Lagrangean code confirm the results of Moskalik, Buchler and Marom (1992) which, we

recall, gave Fourier parameters of the bump Cepheid models that were rather close to the observed values.

Second, it immediately stands out that it is imperative to use a second order scheme for the fluxes, confirming the results of our test examples. We note parenthetically that in a sequence of Cepheid models that we calculated the donor cell fluxes produced results with trends in the amplitude *vs.* period behavior that were completely wrong, even opposite to those both of the higher order scheme and of the purely Lagrangean scheme. For the models calculated with Donor cell advection scheme, the shifts of amplitudes are even opposite for the two choices of handling the energy.

Third, the Fourier parameters exhibit a reasonable robustness when the spatial switchover from Lagrangean to adaptive mesh occurs in the range $j_L=40-60$. Values of $j_L=30$ give already unsatisfactory results. Note also that when the internal energy (IE) equation is solved the Fourier parameters are more sensitive to j_L because of the increased advection errors. This is especially true for the third order radial velocity coefficients R_{31} and ϕ_{31} . This again confirms the numerical superiority of the total energy over the internal energy equation.

Fourth, the adaptive code although requiring some pseudo-viscosity, lets one reduce pseudo-viscous dissipation below values that are possible with the Lagrangean code. The increase of the pulsation amplitude with C_q clearly shows that this amplitude is largely determined by the artificial viscosity independently of the choice of grid. This again illustrates the well known problem that when we reduce the numerical dissipation below the 'standard' values, the pulsation amplitudes get larger than the observed ones (for a discussion *cf. e.g.* Kovács 1990). It must be considered a lucky coincidence that, since the pioneering work of Christy in the 1960s, the use of the 'standard' vNR pseudo-viscosity has yielded pulsation amplitudes in rough agreement with the observed ones. In order to make progress it will be necessary to replace the pseudo-viscous dissipation with the correct physical one, most likely eddy viscosity. It is very likely that the violent shocks induce turbulent motions, especially in the relatively 'soft' (small Γ) partially ionized regions. But to even get a good understanding of where in the star and when in the pulsation phase such turbulent dissipation plays a role, and to get even a crude idea of its magnitude, one needs a 3D hydrodynamic simulation.

Finally, we note that the great advantages of the adaptive numerical calculations is the smoothness of the results. In Figure 7. the temperature variations of the outer 60 shells are shown both for the Lagrangean and for the adaptive results (in both cases as a function of the respective

grid indices). The resolution of the spatial temperature structure is clearly superior by the adaptive mesh.

In Fig. 8 we present the fluid velocity variations of different layers of the model (spread out vertically for clarity), both for the Lagrangean and for the adaptive results. The plotted masses have been selected at the values M_{60}^L , M_{63}^L , $M_{66}^L \dots M_{120}^L$ of the Lagrangean model. In order to compare we have had to interpolate the velocities from the adaptive code for these given values of the masses. The adaptive code is seen to provide significantly smoother curves than the Lagrangean. The relatively sharp features on some of the velocity curves indicate the position of the hydrogen partial ionization front.

Finally, Figure 9 shows the improvement in the quality of the light-curve that is obtained with the adaptive mesh.

4. Conclusion

We have described an adaptive hydrocode which has been specifically developed for stellar pulsation calculations. The code has been tested for shock problems with known analytical solutions. Purposedly, to mimic more realistic calculations in which few mesh points are available for the shock by itself, a relatively coarse mesh has been used. These tests lead to the following conclusions:

- The first order schemes (donor cell) do not give satisfactory agreement between the numerical and analytical solution. At least a second order (*e.g.* van Leer) scheme is necessary.
- The solution of the total energy equation is preferable to the use of an internal energy equation because the numerical deterioration of the results due to the advection errors is reduced.
- A careful application of the adaptive grid technique can provide superior results for tough shock problems even with a relatively few grid points.

It is of course much easier and much faster to run a Lagrangean code than an adaptive one. In particular, the Stellingwerf Lagrangean relaxation method is very efficient when periodic cycles are to be computed as for classical Cepheids or RR Lyrae. The fact that the adaptive mesh can be switched on smoothly starting from a Lagrangean description is therefore a very useful feature.

We have applied the code to a typical Cepheid model pulsator. The temporal variations of the spatial structure of the temperature are well tracked with the adaptive mesh. This results in much smoother velocity and luminosity curves than can be obtained with the Lagrangean code.

Acknowledgements

We are indebted to Géza Kovács for fruitful discussions at the beginning of this project. We also gratefully acknowledge the support of NSF (AST-92-18068), and of an RCI grant by the University of Florida and by IBM at the NERD Center.

References

- Aikawa T. & Simon N. R. 1983, *ApJ* 273, 346
 Alexander, D. R. and Ferguson, J. W. 1994. *ApJ* 437, 879
 Buchler, J. R. 1990, in *The Numerical Modelling of Nonlinear Stellar Pulsations; Problems and Prospects*, Ed. J. R. Buchler, NATO ASI Ser. C302, p. 1 (Dordrecht: Kluwer)
 Buchler, J. R. & Whalen P. 1990, in *The Numerical Modelling of Stellar Pulsations; Problems and Prospects*, Ed. J. R. Buchler, NATO ASI Ser. C302, p. 315 (Dordrecht: Kluwer)
 Castor J. I., Davis C. G. & Davidson D. K. 1977, Los Alamos Sci. Lab. Rep. LA-6664
 Christy R. F. 1966, *Rev. Mod. Phys.* 36, 555
 Cox, A. N., Deupree, R. G. & Gehmeyr, M. 1992, *Physica D*
 Cox, J. P. 1980, *Theory of Stellar Pulsation*, (Princeton: Univ. Press)
 Cox, J. P. & Giuli R. T. 1969, *Principles of Stellar Structure* (New York: Gordon and Breach)
 Dorfi E. A. & Drury L. O. 1987, *J. Comp. Phys.* 69, 175
 Dorfi, E. A. & Feuchtinger, M. U. 1991. *A&A*, 249, 417
 Fraley G. S. 1968, *Ap&SS*, 2, 96
 Feuchtinger, M. U. & Dorfi, E. A. 1994. *A&A*, 291, 209
 Gehmeyr M. 1992a. *ApJ*, 399, 265
 Gehmeyr M. 1992b. *ApJ*, 399, 272
 Gehmeyr M. 1993. *ApJ*, 412, 341
 Iglesias, C. A., Rogers, F. J., Wilson, B. G. 1992, *ApJ* 397, 717
 Kovács, G. 1990, in *The Numerical Modelling of Nonlinear Stellar Pulsations; Problems and Prospects*, Ed. J. R. Buchler, NATO ASI Series C302, p. 53 (Dordrecht: Kluwer).
 Kovács, G. & Buchler, J. R. 1988a, *ApJ*, 324, 1026
 Kovács, G. & Buchler, J. R. 1988b, *ApJ*, 334, 971
 Kovács, G. and Buchler, J. R. 1993. *ApJ* 404, 765
 van Leer, B. 1977. *J. Comp. Phys.* 23, 276
 Moskalik, P., Buchler, J. R. and Marom, A. 1992. *ApJ* 385, 685
 Noh, W. F. 1987. *J. Comp. Phys.* 72, 78.
 Sedov, L. I. 1959 *Similarity and Dimensional Methods in Mechanics* Academic Press, New York.
 Simon N. R. & Aikawa T. 1986, *ApJ* 304, 249
 Stellingwerf R. F. 1974, *ApJ*, 192, 139
 Stellingwerf R. F. 1975, *ApJ* 195, 441 [*cf.* also erratum in *ApJ* 199, 705 (1975)].
 Stobie, R. S. 1969, *MNRAS*, 144, 461
 Winkler K. H. & Norman M. L. 1986, *Astrophysical Radiation Hydrodynamics*, ASI Ser. C, Vol. 188 (Reidel: Dordrecht), p.233

Winkler K. H., Norman M. L. & Mihalas D. 1984, J. Quant. Spectr. Rad. Transf.

| | | | | | | | | | | | | | |
|-------|-------------------|-------|-------------------|---------|-----------|---------------------|-------|---------------------|-----------|---------|-----------|---------------------|-------|
| R_1 | $T_{\frac{3}{2}}$ | R_2 | $T_{\frac{5}{2}}$ | \dots | R_{i-1} | $T_{i-\frac{1}{2}}$ | R_i | $T_{i+\frac{1}{2}}$ | R_{i+1} | \dots | R_{N-1} | $T_{N-\frac{1}{2}}$ | R_N |
| | | | | | | | | | | | | | |
| 1 | | 2 | | | $i-1$ | | i | | $i+1$ | | $N-1$ | | N |
